# Karangkemiri Village Landslide Potential Risk Mapping Based on Integrating Litho-structure and Morphology

FX Anjar Tri Laksono [a,b,*], Muhammad Rifki Fauzan [b], Asmoro Widagdo [b], János Kovács [a]

[a] *Doctoral School of Earth Sciences, Department of Geology and Meteorology, Institute of Geography and Earth Sciences, Faculty of Sciences, University of Pécs, Pécs H-7624, Hungary*

[b] *Geological Engineering Department, Faculty of Engineering, Jenderal Soedirman University, Purbalingga 53371, Indonesia*

*Corresponding author: [*]anjar93@gamma.ttk.pte.hu*

*Abstract*—**The Karangkemiri Village, Jeruklegi District, Cilacap Regency, Central Java Province, has a high risk of rock-mass movement. This is proven by the occurrence of a landslide in March 2020. The susceptibility of landslides is influenced by eight factors: slope, lithology, land cover, elevation, loading, rainfall, distance from rivers, and roads. Therefore, a landslide potential risk map is needed as a disaster mitigation effort. The integration between litho-structure and morphology was applied to understand the distribution of landslides vulnerability in Karangkemiri Village. The Analytical Hierarchy Process (AHP) method was adopted to find the dominant factor that causes a landslide. The result of this study was the geology of a research area consisting of 3 geomorphological units, namely the Structural Curve Slab Hills Unit (S3), Structural Waveed Hills Unit (S2), and Intrusion Unit to Basalt (S11). Stratigraphy of research areas is composed of sandstone (Tmph) and andesite lava (Tmpk) units. Special study methods use the AHP, assessment, and weighting against the landslide movement's causative factors, such calculations combined with primary and secondary data. The data and calculations were inserted into the parameter map then combined to obtain a map of the rock-mass movement susceptibility zone. Analyzing results show research areas divided into two levels of rock-mass movement vulnerability, medium, and high vulnerability levels. Medium levels of vulnerability cover 60% of Karangkemiri Village. Meanwhile, a high level of vulnerability encompasses 40% of Karangkemiri Village.**

*Keywords*—**Susceptibility; litho-structure; landslide, Karangkemiri; Cilacap.**

## I. INTRODUCTION

In March 2020, there was a landslide disaster in Karangkemiri Village, Jeruklegi District, Cilacap Regency, Central Java Province [1], [2]. As an impact of this incident, dozens of houses were slightly damaged. Village infrastructure, such as roads, has also collapsed, making it impossible for car and motorbike drivers to pass [3], [4]. This incident is not the first for Karangkemiri residents, but almost every rainy season, landslides occur, damaging residents' housing and village infrastructure [5]. Karangkemiri Village's location, which is in a paired strike-slip fault zone, reduces slope stability [6], [7]. The two faults are the Muria-Cilacap sinistral fault that traverses northeast-southwest and the Pamanukan-Cilacap dextral fault with a northwest-southeast direction [8], [9]. Both faults are active faults that have the potential to trigger ground movement in Karangkemiri [10]. Human activity like C-mining affects morphological changes

and reduces the stability of the soil structure and slopes [11], [12]. Housing that stands on the fault zone increases the shear force and loading [13]. These problems become the background for mapping the vulnerability level of rock-mass movements in Karangkemiri Village. Research on the potential for landslides in Karangkemiri Village has never been carried out, even though the mapping of landslide-prone zones is needed as a mitigation effort to minimize casualties and material losses.

Landslide potential risk mapping is related to slope stability and soil bearing capacity conditions [14], [15]. In previous studies, slope stability analysis was carried out in three ways of field observation, computation, and graphics [16], [17]. The weakness of field observation is the low level of accuracy and is subjective depending on one's ability to analyze. This method compares an unstable slope to a stable slope. Computing consists of the Fellenius, Bishop, Janbu, and Sarma methods [18], [19]. All computational methods

require data on a slope angle, angle of internal friction, soil shear strength, water table, soil bulk density, cohesion, and unit of weight soil. These parameters are needed to find the slope safety factor [20], [21]. This method is more accurate than field observations but requires more significant cost and time because it requires sampling at the research location and laboratory analysis. In the graphical method, five methods can be used: Taylor, Hoek & Bray, Janbu, Cousins, and Morgenstern [22], [23]. This method is more appropriate for soil that is homogeneous and has a simple structure. Each of the methods used by previous researchers has advantages and disadvantages. Therefore, it is necessary to use a method under the geological conditions and the extensive study area.

The solution proposed in this study is to make a landslide disaster map in Karangkemiri Village by integrating lithology, geological structure, and morphological parameters. The integration represents six factors that cause ground motion: lithology, slope, land cover, elevation, loading, and rainfall. The type of lithology will determine plasticity, cohesion, and permeability, which affect slope stability. The type of lithology also affects the bearing capacity of the soil to withstand loads [24]. Geological structure related to shear forces and rock-mass movement rate. Meanwhile, morphological changes, including slope and elevation, will affect soil shear strength [25]. An assessment of the factors causing landslides in Karangkemiri was conducted to provide executive data for the Cilacap local government in mitigating landslides in Karangkemiri Village.

## II. MATERIALS AND METHOD

To support research activities, the researchers employed some research support tools and materials, as follows:
- Base map of 1:25,000 scale.
- Regional Geology Map scale 1:100,000 Purwokerto-Tegal Research and Development Sheet Center 1309-3 and 1309-6 [26].
- Geological compass.
- Geological hammer (includes a hammer of igneous rocks and a sedimentary rock hammer to sample).
- GPS (Global Positioning System), loupe with 20 X enlargement.
- Comparator large grain and mineral comparator.
- HCl 10%.
- Roll meter.

The activity undertaken next was a surface geological mapping with a scale of 1:25,000 aimed at obtaining primary data that would then be analyzed and processed at the next stage. The details of the activities at this stage among them are geomorphological observations comprising: morphological and landscape observations, straightness patterns indicating structure in research areas, observation of river flow patterns include river genetic type, river valley shape, location, and geographic name as well as the determination of geomorphological units based on Van Zuidam's classification [27], [28]. Next, outcrop observations include outcrop identification covering dimensions, determining the type of lithology, lithology descriptions covering early sedimentology and stratigraphic hypothesis, measurement of elements from a geological structure, data capture of the Strike/Dip layer, as well as sample-taking for laboratory analysis activities [29], [30]. The next step is

acquiring geological structure data, consisting of straightness or brecciation, minor fault mirror, grinding burrow, tensile burrow, and a smear and slope of sedimentary rocks [31], [32]. Then, the researchers continued to take some documentation in plotting stop site locations and temporary track map creation. The next activity is making maps. The data processing stage is done in the studio. At this stage, the work done is to create a map. Maps are created based on surface geological observation data along with their analysis. The map consists of several maps that are modifications to the base map. The maps made between them are:

### A. Geological Track Map

Geological track maps contain information about the location of observation and useful observation pathways to determine lithological units on geological maps. Observation stations and observation lines characterize the lithology encountered in the field. The geological structure measurements and the taking of fossil samples are also listed in those maps [33], [34].

### B. Geomorphological Map

The geomorphological map describes the division of geomorphological units of research areas. The division of such units was based on the results of an analysis of the observed geomorphological data in the field and analysis of contour patterns on the base map [35], [36].

### C. Geological Map

The geological map describes the division of lithological units of research areas and the geological structures acting on research areas [37]. The lithology units' division characterizes rocks' physical characteristics, spread patterns, rock dominance, unit age, and boundaries between units of rock [38]. The geological structure was drawn on the geological map results from analyzing the measurement data of geological structures in the field. It then proceeded with creating the Stratigraphic Column of Research Areas, a sequence model of rock units from old to young on research areas.

### D. Geological Potential Map

The potential map of geological resources contains information regarding geological resources that have economic and prospective value to exploit and some potentially affected areas or inflict a geological disaster, such as flooding, soil movement, and others. Both of these reflect the geological conditions of the research area [39], [40].

### E. Landslide Susceptibility Map

Landslide Susceptibility Map consists of information that has landslide potential or soil movement potential. The ten parameters applied in the landslide susceptibility mapping are slope, soil, lithology, aspect, NDVI, land cover, precipitation, distance to fault, distance to drainage, and road distance. The type of rock-mass movement is identified based on the movement mechanism. The rock-mass movement could be divided into block falls, debris flows, collapses, rock slides, and complex movements [41], [42].

## F. Analytical Hierarchy Process (AHP) Method

This study used the analytical hierarchy process (AHP) method: assessment and weighting from the main parameters to resolve the complex multicriteria problem into a hierarchy, Saaty. The parameters valued in this study are slope, lithology, weathering of rocks, and land use. Data from each parameter in the group (subparameter) uses data derived from primary and secondary data. Assessment of the main parameters is done based on the parameter importance level table (Table I), then displayed in pairwise comparison matrices. Each parameter's assessment and weighting methods were performed to obtain quantitative results to state the threat index most influential in the research area [43]. GIS-raster is adopted to calculate the effect of criteria and sub-criteria. The use of landslide location plots in Karangkemiri was carried out to validate the analysis results [44]–[46].

TABLE I
THE PREFERENCE LEVELS OF MULTIPLE ALTERNATIVES IN THE PAIRWISE

| Intensity of Importance | Definition |
|---|---|
| 1 | Equal importance |
| 2 | Weak |
| 3 | Moderate importance |
| 4 | Moderate plus |
| 5 | Strong importance |
| 6 | Strong plus |
| 7 | Very strong or demonstrated importance |
| 8 | Very, very strong |
| 9 | Extreme importance |

Each parameter's weight is said to be either or consistent when it has a CR value of <0.1. The value of CI and CR can be calculated using the equation 1 and 2 [48], [49]:

$$CI = \frac{(?\max - n)}{n - 1} \qquad (1)$$

$$CR = \frac{(CI)}{RI} \qquad (2)$$

CI $\qquad$ = Consistency Index
λ maks $\qquad$ = Maximum eigenvalue
n $\qquad$ = The number of parameters
RI $\qquad$ = Ratio index
CR $\qquad$ = Consistency ratio

Maximum lamda is obtained by multiplying pairwise comparison matrices with each parameter's weight, while Ratio index is obtained from Ratio Index Table (see Table II).

TABLE II
THE VALUE OF RANDOM INDEX (RI) DEPENDS ON THE N-MATRIX

| N | RI |
|---|---|
| 1 | 0 |
| 2 | 0 |
| 3 | 0.58 |
| 4 | 0.90 |
| 5 | 1.12 |
| 6 | 1.24 |
| 7 | 1.32 |
| 8 | 1.41 |
| 9 | 1.45 |
| 10 | 1.49 |
| 11 | 1.48 |
| 12 | 1.51 |
| 13 | 1.56 |
| 14 | 1.57 |
| 15 | 1.59 |

## G. Geographic Information System (GIS)

The creation of soil motions vulnerability zoning map used ArcGIS software because it can connect various data at a given point on earth, combine them, analyze and eventually map. First, Switch map data every parameter to be used in the ArcGIS layer. Next, Either parameter map enters the grade value, weight value, and score value used, by right-clicking on the parameter map, then click the open attribute table, and enter the value. After that, create a new layer in a way, on ArcToolbox then select and click Analysis Tools > Overlay > Union. Enter the parameters to use on Input Features [52].

After the finished layer union is processed, right-click on the layer union, select the attribute table. Next, add Field "total score" for each parameter's total score, then select Type "Double". Next, Calculates that total score by right-clicking on the total score field, then click 'kalkulator lapangan' [53]. Change colors based on the total score by right-clicking, select Properties, click Symbology, and select Quantities. A map that is overlayed at this stage results in a map of the soil motion vulnerability zone. The s proselytization map is divided into two tiers, which refer to Indonesian National Standard [54].

## H. Research Flow Chart

Determination of the rock-mass movement vulnerability zone begins with a literature review to find out how far previous research is related to the mapping of soil movement vulnerability zones, especially using the AHP method. The study area's regional geological structure and stratigraphy are needed to obtain faults and rock formations data that may be present in the study area. The initial hypothesis depicts that lithology and geological structure greatly influence the landslide potential risk. Combining these two parameters with morphological data is likely to increase the landslide potential risk map's accuracy. Karangkemiri Village is selected to prove this hypothesis. The location selection is based on the landslide history, the complexity of lithology and geological structures, varied morphology, and the absence of a landslide potential risk map in Karangkemiri Village. The field data collection includes geomorphological conditions, the study area's lithology composition, slope stability, and geological structures. Secondary data collected consisted of regional geology and SRTM imagery.

Field and secondary data processing results are geological maps, slope stability maps, and geomorphological maps. Implementing the AHP method begins with creating a hierarchy to determine the main objectives and parameters input. The parameters included in this study consisted of lithology, geological structure, and morphology. Using the relative importance scale, the parameter importance value is determined at the comparison matrix creation stage. Consistency ratio calculation is applied to verify decisions that have been made—evaluation of the consistency ratio using the Eigenvector Saaty method. If the consistency ratio (CR) is less than 0.1 then the decision is accepted. However, if CR is more than 0.1 then the decision is rejected, and the comparison matrix must be made again. Overlay between geological, geomorphological, and slope stability maps will give an output in the form of a landslide susceptibility map (Fig.1).
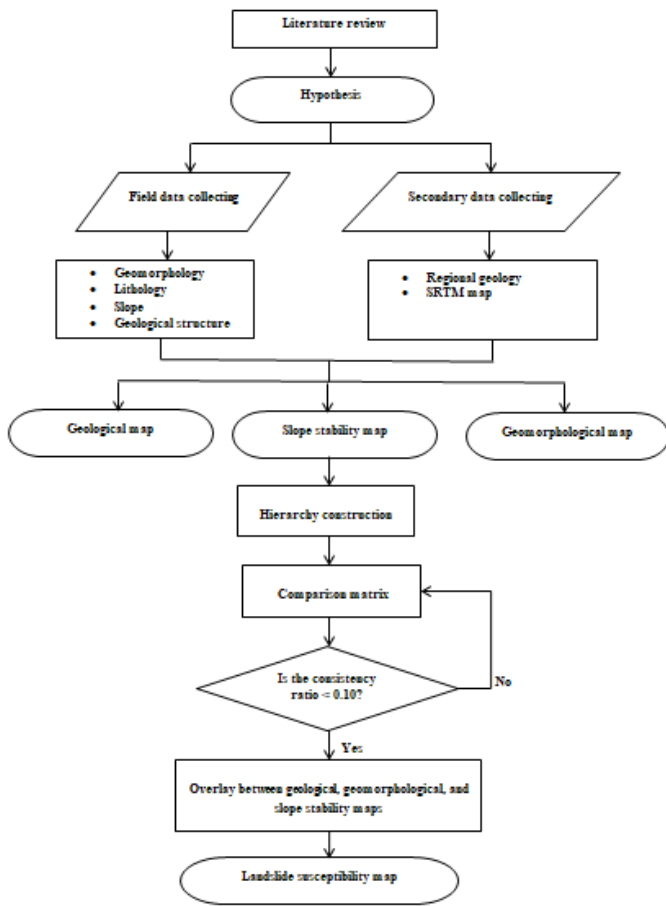
Fig. 1 Flow chart of landslide potential risk mapping in Karangkemiri Village.

## III. RESULTS AND DISCUSSION

### A. Geomorphological Research Area

The research area is divided into three geomorphological units based on the Van Zuidam classification [55], namely structural curve slab hills unit, structural waved hills unit, intrusion unit to basalt (Fig. 2).
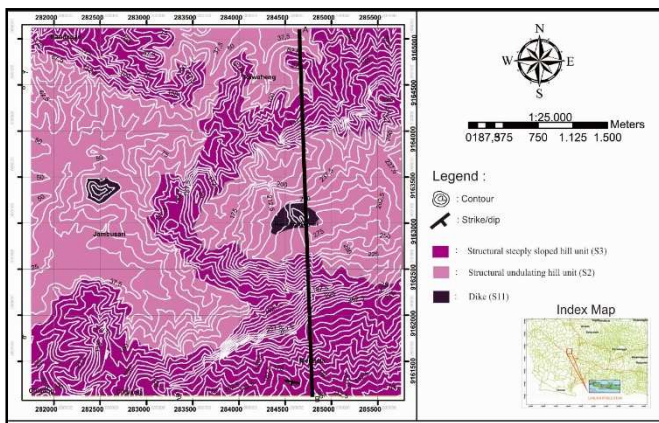


Fig. 2 Geomorphological map of the research area. The dark purple color for structural curve slab hills unit, bright purple for structural waved hills unit, and the darkest purple for intrusion unit to basalt.

### B. Structural Curve Slab Hills Unit

This geomorphological unit encompasses 54% of the overall research area. This unit is characterized by dark purple

color on the northern and eastern parts (Fig. 2). It is marked by the imperatively bumpy contour and the slope relative to the north. This structural curve slab hills unit has contours inclined to tightly, 62.5 m–275 m above sea level with a contour elevation of 212.5 m. The unit is a hill with an average slope of 58% using the Van Zuidam slope classification [28] being on a steep mountain (Table III).

### C. Structural Waveed Hills Unit

This geomorphological unit includes 45% of the overall research area. On geomorphological maps are characterized by very young purple colors on the southern and western parts (Fig. 2). It is marked by the valley's prune (Fig. 3), and the slope is categorized gentle to the tilted towards the west-east. This structural wavy low hill unit has a contour tending to the rim, being at elevation 25-87.5 m above sea level (masl) with an elevation of 100 m. This structural wavy low hills unit has a contour tending to the rim, being at elevation 25-87.5 m above sea level (masl) with 100 m. this unit constitutes a valley with an average slope of 22% and, based on the Van Zuidam classification [56], being on hilly to mountainous (Table III).

### D. Intrusion Unit to Basalt

This geomorphological unit covers 1% of the overall research area. The darkest purple color marks this unit on the central part of the map (Fig. 2). It is marked by the intrusion impairment of igneous rocks that have columnar joint-like structures. This unit Dike has a relative contour of slack-meeting, being at elevation 237.5 m–275 m above sea level (Table III). The average slope percentage is 60% which is included in the steep mountain according to the Van Zuidam classification.
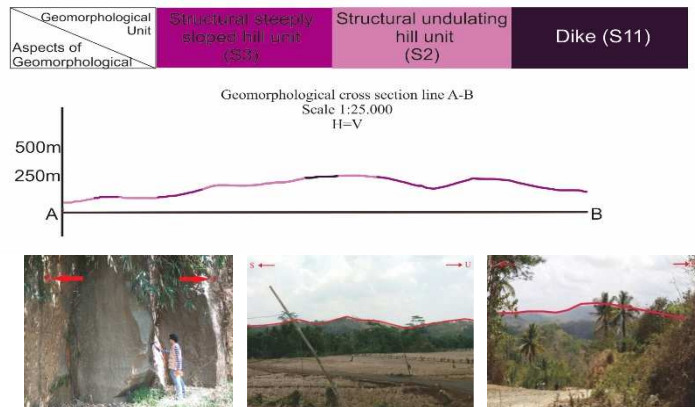


Fig. 3 The relationship between morphological units, geomorphological profiles, and landform appearance in the field.

TABLE III
THE SLOPE PERCENT AVERAGE IN KARANGKEMIRI VILLAGE SHOWS HILLY TO STEEP MOUNTAIN

| Slope Percent Average | Highest Point | Lowest Point | Different Height |
|---|---|---|---|
| 58% | 275 masl | 62.5 masl | 212.5 masl |
| 22% | 87.5 masl | 25 masl | 62.5 masl |
| 60% | 275 masl | 237.5 masl | 37.5 masl |

There are two types of rivers in Karangkemiri Village, namely parallel and dendritic. The parallel flow pattern is characterized by parallels between rivers, most of which are

on steep slopes. Meanwhile, the dendritic river flow type reflects the rock resistance. The more resistant the rocks, the more tenuous river flow patterns are formed. The valley shape in the parallel river flow type is V, while the valley shape in the dendritic river flow type is U (Table IV).

TABLE IV
THE TWO TYPES OF RIVERS IN THE KARANGKEMIRI VILLAGE ARE PARALLEL AND DENDRITIC WITH THE V AND U VALLEY SHAPE

| Type of River | Valley Shape | Lithology | Land Use |
|---|---|---|---|
| Parallel | V | Sandstone, claystone | Rice field, settlement, plantation |
| Dendritic | U | Sandstone, claystone | Rice field, settlement, plantation |
| - | - | Basalt intrusion | Plantation |

The endogenous process in Karangkemiri Village is caused by tectonism which causes geological structures in the form of faults and folds. Besides, the presence of basalt intrusion in the form of sill and dike indicates volcanism. Exogenous destructive processes such as weathering, and erosion remove some of the traces of endogenous processes (Table V).

TABLE V
ENDOGENIC PROCESSES ARE DOMINATED BY TECTONISM, WHICH CAUSES FAULTS AND FOLDS. MEANWHILE, THE EXOGENIC PROCESSES THAT OCCUR IN KARANGKEMIRI VILLAGE ARE WEATHERING AND EROSION

| Endogenic Process | Exogenic Process | Geological Structure |
|---|---|---|
| Joint, fault, fold | Weathering, erosion, sedimentation | Fault, fold |
| Joint, fault, fold | Weathering, erosion, sedimentation | Fault, fold |
| Basalt intrusion | Weathering, erosion | Sill, dike |

## E. Geological Map

Based on observational data and research of conditions in the field and laboratory analysis results, the research area can be grouped into two rock units that are sandstone-staffed clay intersection unit and intrusion basalt (Fig. 4).
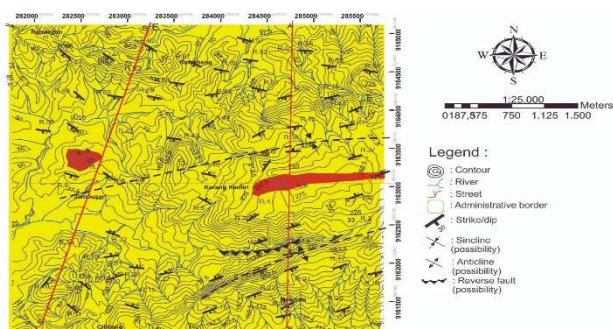


Fig. 4 Geological map of the research area. The yellow color for representing of Sandstone-staffed Clay Intersection Unit and red color for Intrusion Basalt

The dominant differences in lithological characteristics in the research area became the basis of the division of rock units in mapping areas, following units of rock present in mapping areas, sorted from old to young. Based on the geological profile, the sandstone units are deposited first, then tectonism occurs, which results in the formation of anticlines. A thrust fault then deforms the anticline. Basalt intrusion is formed after the deformation of the sandstone unit (Fig. 5).
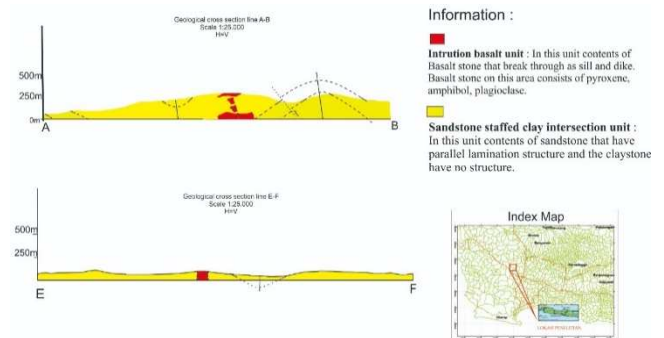


Fig. 5 Section A-B and E-F of the research area's geological map illustrate the sandstone staffed clay intersection unit older than the basalt intrusion unit.

## F. Sandstone-staffed Clay Intersection Unit

The sandstone-staffed clay intersection unit is marked in yellow on the geological map. This unit occupies ± 95% of the study area. The outcrop on this unit was found in the study area which was exposed in fresh to highly weathered rock. This lithological unit is found in highly weathered rock conditions. This lithology unit's thickness based on calculations and analysis on the geological profile is about 907.5 m. This is interpreted as the oldest lithological unit because the rock layer's dip direction is away from this lithological unit.

## G. Intrusion Basalt

The basalt intrusion unit is marked in red on the geological map, which occupies ± 5% of the study area. The outcrop on this unit was found in the central area of the Karangkemiri Village exposed in highly weathered rock. The thickness of this lithology is estimated at 250 m. It is younger than the Sandstone-staffed clay intersection unit because it approaches the dip direction of the layer.

## H. Percent Slope Map

This map describes that the slope is expressed as a percent. This map is created based on the classification of Van Zuidam (Fig. 6). Karangkemiri village is dominated by a slope of 30% -140% which is included in the steep to very steep category. On the map Fig. 6, the area is indicated in pink to red.
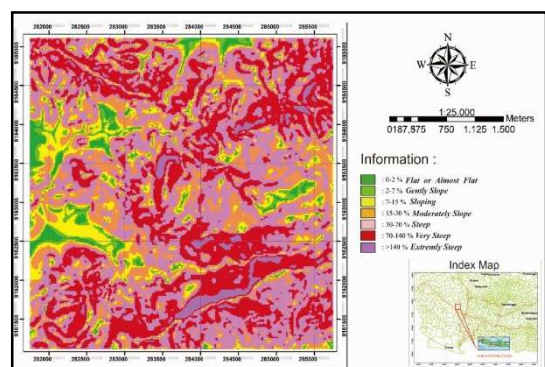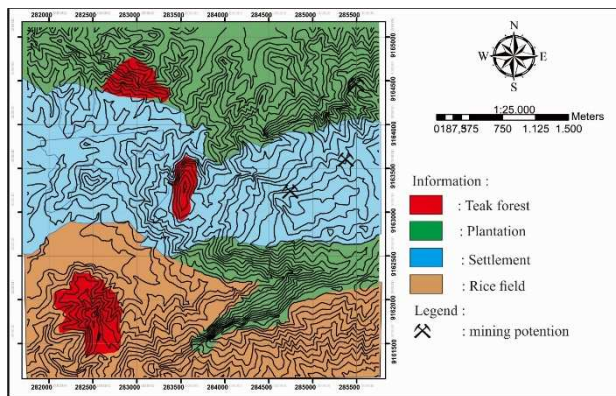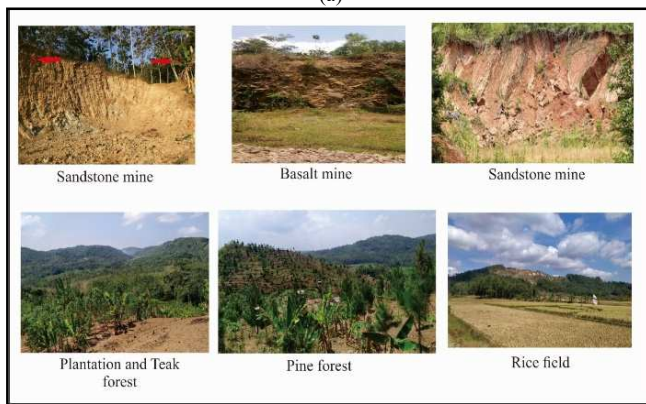


Fig. 6 The Karangkemiri Village slope is dominated by steep to very steep based on the Van Zuidam classification.

## I. Land Use Map

The land use of Karangkemiri Village consists of 4 units. There are for the teak forest, plantation, settlement, and rice fields. Then, the geological potential in this research area encompasses sandstone and basalt mine (Fig. 7).



(a)



(b)

Fig. 7 (a) The red color represents the teak forest, green for plantation, blue is settlement, and rice fields are illustrated as brown. b) The mining of sandstone and basalt induce gentle slopes to be steep slopes.

## J. Landslide Susceptibility Map

For make a landslide susceptibility map, needs some parameters for the process. Unique study methods use the Analytical Hierarchy Process (AHP), assessing and weighing against soil movement's causative factors, such as calculations combined with primary and secondary data. The data and calculations are inserted into the parameter map then overgrown (overlay) so that a map of the soil motion susceptibility zone is obtained. In this research, the parameters used are geological, slope, and geomorphological map. Sandstone is a sediment rock type that has good porosity and good permeability. Therefore, this lithology can quickly turn into soil and prone to soil movement due to reduced shear strength (Table VI). Basalt has poor permeability, poor porosity but has good resistance. Here is the table of lithology ratios.

TABLE VI
THE SUB-PARAMETER RATIO OF LITHOLOGY DEPICTS THAT SEDIMENTARY ROCK HAS A HIGHER VALUE THAN BASALT

| Lithology | Value | Class |
|---|---|---|
| Sediments | 2 | High |
| Basalt | 1 | Low |

The slope is one of some parameters that are very important because the slope is representing the morphological elevation on the research area (Table VII).

TABLE VII
THE SUB-PARAMETER RATIO OF SLOPE

| Slope | Value | Class |
|---|---|---|
| 0-15 | 1 | Low |
| 15-70 | 2 | Mid |
| >70 | 3 | High |

Land use in the research area has an impact on the soil movement in the research area. Land use may increase the burden a lithology must bear and reduce the slope stability level to trigger the avalanche (Table VIII).

TABLE VIII
THE SUB-PARAMETER RATIO OF LAND USE

| Land Use | Value | Class |
|---|---|---|
| Teak Forest | 1 | Low |
| Plantation | 2 | Mid |
| The settlement, rice fields | 3 | High |

A zoning map of soil motion susceptibility in the research area was generated through overlapping (overlay) processes of each parameter map that has been scored. The map overlay process is created using the help of ArcGIS software. The map of the soil motion susceptibility zone coupled with the threat point of ground motion was found at the research site. There were as many as 5 points of the threat of ground movement at the research site with relatively similar levels of vulnerability (Table IX).

TABLE IX
THE SUB-PARAMETER RATIO OF LAND USE

| Parameter | N1 | N2 | N3 |
|---|---|---|---|
| N1 | 1 | 0,5 | 2 |
| N2 | 2 | 1 | 3 |
| N3 | 0.5 | 0,333333 | 1 |
| Total | 3.5 | 1.833333 | 6 |

Pairwise matrix comparisons of the 3 parameters entered are then added and weighted to obtain a consistency ratio (Table X)

TABLE X
COUPLE MATRIX RATIO OF PARAMETERS NORMALIZED

| Parameter | N1 | N2 | N3 | SUM | Weight |
|---|---|---|---|---|---|
| N1 | 0.28571 | 0.27272 | 0.33333 | 0.89177 | 0.29725 |
| N2 | 0.57142 | 0.54545 | 0.5 | 0.61688 | 0.53896 |
| N3 | 0.14285 | 0.18181 | 0.16667 | 0.49134 | 0.16378 |
| Total | | | | 3 | 1 |

The weight of each parameter is said to be either or consistent when it has a CR value of <0.1. The value of C1 and CR can be calculated using the equation 1 and 2:

Known:
EIGEN MAX = 3,011183
N = 3
RI = 0,58

$$CI = \frac{(\lambda\max - n)}{n - 1} \qquad (1)$$

$$CI = \frac{(3{,}011183 - 3)}{3 - 1}$$

$$CI = 0{,}005592$$

$$CR = \frac{(CI)}{RI} \qquad (2)$$

$$CR = \frac{(3{,}011183 - 3)}{3 - 1}$$

$$CR = \frac{0{,}005592}{0{,}58}$$

$$CR = 0{,}009641$$

Next, the scores of soil motion susceptibility levels in Karangkemiri Village can be gained from the calculation result of the ground motion threat factor's parameter weight multiplied by the sub-parameter class of ground motion threat (Fig. 8).
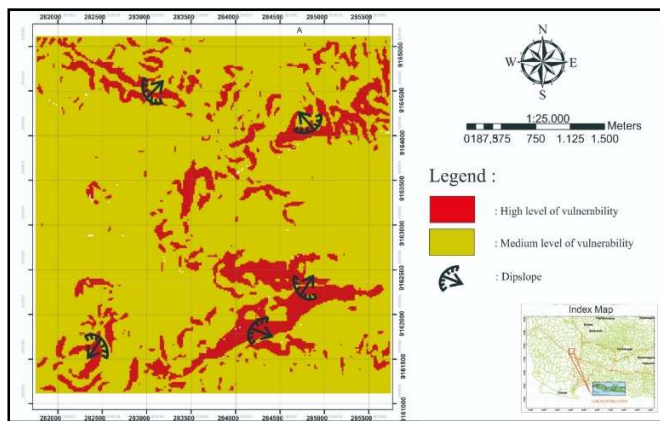


Fig. 8 Landslide susceptibility map of Karangkemiri Village. The red color represents high levels of vulnerability and the brown color displays medium levels of vulnerability.

### K. Medium Level of Vulnerability

The medium level of vulnerability zone occupies 60% of the entire research site. It is dominated by gently sloping to moderately steep. The slope constituent lithology is in the form of sandstones with diverse rock weathering conditions fresh to residual soil. Land use in this zone is in plantations, settlements, rice fields, and forest areas. In this zone, there are two ground motion threat points.

### L. High level of vulnerability

The zone occupies 40% of the entire research site. It is dominated by the strongly sloping to very steep, thus causing this area to enter the high ground movement threat level. The slope constituent lithology is in the form of sandstones with diverse rock weathering conditions fresh to residual soil. Land use in this zone is in plantations, settlements, rice fields, and forest areas. In this zone, we found 3 ground motion threat points.

## IV. CONCLUSION

In this study, two soil movement vulnerability zones are found in medium-level movement zones in research areas that occupy 60% of the entire research site, and high-level movement zones occupy 40% of the entire research area. Landslide potential in research areas occur and form due to steep slope slanting factors, then supported by the morphology of research areas and the blossomed lithology of research areas. Steep slope states and abundant dominance of sedimentary rocks in the research area are particularly possible to accelerate the rate of motion of the soil when a landslide occurs. This is because sedimentary rocks have good porosity and permeability to pass water. The steep slope is the most influential factor in the zoning of the research area's soil movement. Then in sequence continued with another factor, namely rock weathering, slope constituent lithology, and less suitable land use.

## REFERENCES

[1] E. Gunawan and S. Widiyantoro, "Active tectonic deformation in Java, Indonesia inferred from a GPS-derived strain rate," *J. Geodyn.*, 2019, doi: 10.1016/j.jog.2019.01.004.

[2] W. Fan, D. Bassett, J. Jiang, P. M. Shearer, and C. Ji, "Rupture evolution of the 2006 Java tsunami earthquake and the possible role of splay faults," *Tectonophysics*, 2017, doi: 10.1016/j.tecto.2017.10.003.

[3] N. D. Hananto *et al.*, "Tsunami earthquakes: Vertical pop-up expulsion at the forefront of subduction megathrust," *Earth Planet. Sci. Lett.*, 2020, doi: 10.1016/j.epsl.2020.116197.

[4] M. R. Daryono, D. H. Natawidjaja, B. Sapiie, and P. Cummins, "Earthquake Geology of the Lembang Fault, West Java, Indonesia," *Tectonophysics*, 2019, doi: 10.1016/j.tecto.2018.12.014.

[5] Suwarno, Misnah, and Mujiarto, "Analysis of static morphostructure conditions with dynamic morfostructure (Landslide type)," *Geogr. Tech.*, 2020, doi: 10.21163/GT_2020.151.06.

[6] S. K. Suhardja, S. Widiyantoro, J. P. Métaxian, N. Rawlinson, M. Ramdhan, and A. Budi-Santoso, "Crustal thickness beneath Mt. Merapi and Mt. Merbabu, Central Java, Indonesia, inferred from receiver function analysis," *Phys. Earth Planet. Inter.*, 2020, doi: 10.1016/j.pepi.2020.106455.

[7] G. I. Marliyani, H. Helmi, J. R. Arrowsmith, and A. Clarke, "Volcano morphology as an indicator of stress orientation in the Java Volcanic Arc, Indonesia," *J. Volcanol. Geotherm. Res.*, 2020, doi: 10.1016/j.jvolgeores.2020.106912.

[8] A. Koulali *et al.*, "The kinematics of crustal deformation in Java from GPS observations: Implications for fault slip partitioning," *Earth Planet. Sci. Lett.*, 2017, doi: 10.1016/j.epsl.2016.10.039.

[9] E. Oral, H. Weng, and J. P. Ampuero, "Does a Damaged-Fault Zone Mitigate the Near-Field Impact of Supershear Earthquakes?—Application to the 2018 Mw 7.5 Palu, Indonesia, Earthquake," *Geophys. Res. Lett.*, 2020, doi: 10.1029/2019GL085649.

[10] F. Guzzetti *et al.*, "Geographical landslide early warning systems," *Earth-Science Reviews*. 2020, doi: 10.1016/j.earscirev.2019.102973.

[11] H. A. Nefeslioglu and T. Gorum, "The use of landslide hazard maps to determine mitigation priorities in a dam reservoir and its protection area," *Land use policy*, 2020, doi: 10.1016/j.landusepol.2019.104363.

[12] M. Shafique, "Spatial and temporal evolution of co-seismic landslides after the 2005 Kashmir earthquake," *Geomorphology*, 2020, doi: 10.1016/j.geomorph.2020.107228.

[13] Y. Pan, G. Wu, Z. Zhao, and L. He, "Analysis of rock slope stability under rainfall conditions considering the water-induced weakening of rock," *Comput. Geotech.*, 2020, doi: 10.1016/j.compgeo.2020.103806.

[14] Q. Lv, Y. Liu, and Q. Yang, "Stability analysis of earthquake-induced rock slope based on back analysis of shear strength parameters of rock mass," *Eng. Geol.*, 2017, doi: 10.1016/j.enggeo.2017.07.007.

[15] Y. Tang *et al.*, "Integrating principal component analysis with statistically-based models for analysis of causal factors and landslide susceptibility mapping: A comparative study from the loess plateau area in Shanxi (China)," *J. Clean. Prod.*, 2020, doi: 10.1016/j.jclepro.2020.124159.

[16] M. F. Barchia, "Options for Land Conservation Practices Based on Land Uses in Kungkai Watershed, Bengkulu, Sumatera, Indonesia," *Int. J. Environ. Sci. Dev.*, 2016, doi: 10.7763/ijesd.2016.v7.772.

[17] H. Han, B. Shi, and L. Zhang, "Prediction of landslide sharp increase displacement by SVM with considering hysteresis of groundwater change," *Eng. Geol.*, 2020, doi: 10.1016/j.enggeo.2020.105876.

[18] D. Rohit, S. M. K. Pasha, H. Hazarika, T. Kokusho, A. Arsyad, and S. Nurdin, "Influence of low permeability capping layers on liquefaction induced ground failure," 2020.

[19] P. Schlotfeldt, D. Elmo, and B. Panton, "Overhanging rock slope by design: An integrated approach using rock mass strength characterisation, large-scale numerical modelling and limit equilibrium methods," *J. Rock Mech. Geotech. Eng.*, 2018, doi: 10.1016/j.jrmge.2017.09.008.

[20] P. Zhou and S. Xia, "Effects of the heterogeneous subducting plate on seismicity: Constraints from b-values in the Andaman–Sumatra–Java subduction zone," *Phys. Earth Planet. Inter.*, 2020, doi: 10.1016/j.pepi.2020.106499.

[21] R. Paris, K. Goto, J. Goff, and H. Yanagisawa, "Advances in the study of mega-tsunamis in the geological record," *Earth-Science Reviews*. 2020, doi: 10.1016/j.earscirev.2020.103381.

[22] K. Pawluszek, "Landslide features identification and morphology investigation using high-resolution DEM derivatives," *Nat. Hazards*, 2019, doi: 10.1007/s11069-018-3543-1.

[23] K. Pawłuszek, S. Marczak, A. Borkowski, and P. Tarolli, "Multi-aspect analysis of object-oriented landslide detection based on an extended set of LiDAR-derived terrain features," *ISPRS Int. J. Geo-Information*, 2019, doi: 10.3390/ijgi8080321.

[24] M. Panahi, A. Gayen, H. R. Pourghasemi, F. Rezaie, and S. Lee, "Spatial prediction of landslide susceptibility using hybrid support vector regression (SVR) and the adaptive neuro-fuzzy inference system (ANFIS) with various metaheuristic algorithms," *Sci. Total Environ.*, 2020, doi: 10.1016/j.scitotenv.2020.139937.

[25] S. Truttmann, M. Herwegh, G. Schreurs, A. Ebert, and S. Hardmeier, "The Effect of Pre-Existing Structures on the Moosfluh Landslide and its Lateral Propagation (Great Aletsch Glacier, Switzerland)," *Geomorphology*, 2020, doi: 10.1016/j.geomorph.2020.107530.

[26] E. Gunawan, I. Meilano, N. R. Hanifa, and S. Widiyantoro, "Effect of coseismic and postseismic deformation on homogeneous and layered half-space and spherical analysis: Model simulation of the 2006 Java, Indonesia, tsunami earthquake," *J. Appl. Geod.*, 2017, doi: 10.1515/jag-2017-0009.

[27] Z. Li, Q. Liu, H. Zhu, X. Zhang, M. Li, and Q. Zhao, "Compositional relationship between the source-to-sink segments and their sedimentary response to diverse geomorphology types in the intrabasinal lower uplift of continental basins," *Mar. Pet. Geol.*, 2021, doi: 10.1016/j.marpetgeo.2020.104716.

[28] S. L. Gallop *et al.*, "Geologically controlled sandy beaches: Their geomorphology, morphodynamics and classification," *Science of the Total Environment*. 2020, doi: 10.1016/j.scitotenv.2020.139123.

[29] M. K. Khalifa and K. J. Mills, "Facies analysis relationships depositional environments of the subsurface stratigraphy of the Snake Cave Interval in the Bancannia Trough, western Darling Basin, New South Wales, SE Australia," *Mar. Pet. Geol.*, 2020, doi: 10.1016/j.marpetgeo.2020.104274.

[30] A. Giri, R. Anand, S. Balakrishnan, J. K. Dash, and D. S. Sarma, "Neoarchean magmatism in Shimoga greenstone belt, India: Evidence for subduction-accretion processes in the evolution of the western Dharwar stratigraphy," *Lithos*, 2019, doi: 10.1016/j.lithos.2019.02.015.

[31] A. Bischoff, M. Schleiting, R. Wieler, and M. Patzek, "Brecciation among 2280 ordinary chondrites – Constraints on the evolution of their parent bodies," *Geochim. Cosmochim. Acta*, 2018, doi: 10.1016/j.gca.2018.07.020.

[32] J. L. H. Cailteux, P. Muchez, J. De Cuyper, S. Dewaele, and T. De Putter, "Origin of the megabreccias in the Katanga Copperbelt (D.R.Congo)," *J. African Earth Sci.*, 2018, doi: 10.1016/j.jafrearsci.2017.12.029.

[33] F. E. Gruber, J. Baruck, V. Mair, and C. Geitner, "From geological to soil parent material maps - A random forest-supported analysis of geological map units and topography to support soil survey in South Tyrol," *Geoderma*, 2019, doi: 10.1016/j.geoderma.2019.113884.

[34] A. Beniest and W. P. Schellart, "A geological map of the Scotia Sea area constrained by bathymetry, geological data, geophysical data and seismic tomography models from the deep mantle," *Earth-Science Reviews*. 2020, doi: 10.1016/j.earscirev.2020.103391.

[35] M. B. González, D. Rodríguez-Oroz, J. Alcalá-Reygosa, and N. Campos, "Geomorphological mapping and landforms characterization of a high valley environment in the Chilean Andes," *J. South Am. Earth Sci.*, 2020, doi: 10.1016/j.jsames.2020.102918.

[36] T. Oguchi, "Geomorphological debates in Japan related to surface processes, tectonics, climate, research principles, and international geomorphology," *Geomorphology*, 2020, doi: 10.1016/j.geomorph.2019.06.019.

[37] C. Wang, X. Ma, and J. Chen, "Ontology-driven data integration and visualization for exploring regional geologic time and paleontological information," *Comput. Geosci.*, 2018, doi: 10.1016/j.cageo.2018.03.004.

[38] J. Guo *et al.*, "Explicit-implicit-integrated 3-D geological modelling approach: A case study of the Xianyan Demolition Volcano (Fujian, China)," *Tectonophysics*, 2020, doi: 10.1016/j.tecto.2020.228648.

[39] S. Moretto, F. Bozzano, C. Esposito, P. Mazzanti, and A. Rocca, "Assessment of landslide pre-failure monitoring and forecasting using satellite SAR interferometry," *Geosci.*, 2017, doi: 10.3390/geosciences7020036.

[40] Y. Zhang *et al.*, "Forecasting the magnitude of potential landslides based on InSAR techniques," *Remote Sens. Environ.*, 2020, doi: 10.1016/j.rse.2020.111738.

[41] S. Saha *et al.*, "Prediction of landslide susceptibility in Rudraprayag, India using novel ensemble of conditional probability and boosted regression tree-based on cross-validation method," *Sci. Total Environ.*, 2020, doi: 10.1016/j.scitotenv.2020.142928.

[42] A. M. Youssef and H. R. Pourghasemi, "Landslide susceptibility mapping using machine learning algorithms and comparison of their performance at Abha Basin, Asir Region, Saudi Arabia," *Geosci. Front.*, 2020, doi: 10.1016/j.gsf.2020.05.010.

[43] D. Sun, H. Wen, D. Wang, and J. Xu, "A random forest model of landslide susceptibility mapping based on hyperparameter optimization using Bayes algorithm," *Geomorphology*, 2020, doi: 10.1016/j.geomorph.2020.107201.

[44] L. Lombardo and H. Tanyas, "Chrono-validation of near-real-time landslide susceptibility models via plug-in statistical simulations," *Eng. Geol.*, 2020, doi: 10.1016/j.enggeo.2020.105818.

[45] I. G. Tunas and R. Maadji, "The use of GIS and hydrodynamic model for performance evaluation of flood control structure," *Int. J. Adv. Sci. Eng. Inf. Technol.*, 2018, doi: 10.18517/ijaseit.8.6.7489.

[46] M. F. Barchia, K. Amri, and R. Apriantoni, "Land Degradation and Option of Practical Conservation Concepts in Manna Watershed Bengkulu Indonesia," *TERRA J. L. Restor.*, 2019, doi: 10.31186/terra.1.2.23-30.

[47] A. Arabameri, B. Pradhan, K. Rezaei, M. Sohrabi, and Z. Kalantari, "GIS-based landslide susceptibility mapping using numerical risk factor bivariate model and its ensemble with linear multivariate regression and boosted regression tree algorithms," *J. Mt. Sci.*, 2019, doi: 10.1007/s11629-018-5168-y.

[48] M. E. Fauzan, A. Damayanti, and R. Saraswati, "Vulnerability assessment of landslide areas in Ci Manuk Upstream Watershed, Garut District, West Java Province," *Int. J. Adv. Sci. Eng. Inf. Technol.*, 2020, doi: 10.18517/ijaseit.10.1.6755.

[49] I. G. Tunas, A. Tanga, and S. R. Oktavia, "Impact of landslides induced by the 2018 palu earthquake on flash flood in bangga river Basin, Sulawesi, Indonesia," *J. Ecol. Eng.*, 2020, doi: 10.12911/22998993/116325.

[50] P. T. Thi Ngo *et al.*, "Evaluation of deep learning algorithms for national scale landslide susceptibility mapping of Iran," *Geosci. Front.*, 2020, doi: 10.1016/j.gsf.2020.06.013.

[51] D. Bălteanu *et al.*, "National-scale landslide susceptibility map of Romania in a European methodological framework," *Geomorphology*, 2020, doi: 10.1016/j.geomorph.2020.107432.

[52] D. Tien Bui *et al.*, "Spatial prediction of rainfall-induced landslides for the Lao Cai area (Vietnam) using a hybrid intelligent approach of least squares support vector machines inference model and artificial bee colony optimization," *Landslides*, 2017, doi: 10.1007/s10346-016-0711-9.

[53] B. T. Pham, D. Tien Bui, and I. Prakash, "Landslide Susceptibility Assessment Using Bagging Ensemble Based Alternating Decision Trees, Logistic Regression and J48 Decision Trees Methods: A Comparative Study," *Geotech. Geol. Eng.*, 2017, doi: 10.1007/s10706-017-0264-2.

[54] B. T. Pham *et al.*, "GIS-based ensemble soft computing models for landslide susceptibility mapping," *Adv. Sp. Res.*, 2020, doi: 10.1016/j.asr.2020.05.016.

[55] A. Milia, P. Iannace, and M. M. Torrente, "Active tectonic structures and submarine landslides offshore southern Apulia (Italy): A new scenario for the 1743 earthquake and subsequent tsunami," *Geo-Marine Lett.*, 2017, doi: 10.1007/s00367-017-0493-7.

[56] A. Anugrahadi, U. Sumotarto, and T. T. Purwiyono, "Geomorphological impact of Palu earthquake," 2019, doi: 10.1088/1742-6596/1402/3/033015.